

# 3C 295, A CLUSTER AND ITS COOLING FLOW AT Z=0.46

D.M. Neumann

CEA/Saclay, Service d'Astrophysique, Orme des Merisiers, Bât. 709, 91191 Gif-sur-Yvette Cedex, France  
Max-Planck-Institut für extraterrestrische Physik, Giessenbachstr. 1 D-85740 Garching, Germany,  
email:ddon@cea.fr

## ABSTRACT

We present ROSAT HRI data of the distant and X-ray luminous ( $L_x(bol) = 2.6_{-0.2}^{+0.4} \times 10^{45}$  erg/sec) cluster of galaxies 3C 295. We fit both a one-dimensional and a two-dimensional isothermal  $\beta$ -model to the data, the latter one taking into account the effects of the point spread function (PSF). For the error analysis of the parameters of the two-dimensional model we introduce a Monte-Carlo technique.

Applying a substructure analysis, by subtracting a cluster model from the data, we find no evidence for a merger, but we see a decrement in emission South-East of the center of the cluster, which might be due to absorption.

We confirm previous results by Henry & Henriksen (1986) that 3C 295 hosts a cooling flow. The equations for the simple and idealized cooling flow analysis presented here are solely based on the isothermal  $\beta$ -model, which fits the data very well, including the center of the cluster. We determine a cooling flow radius of 60–120 kpc and mass accretion rate of  $\dot{M} = 400 - 900 M_{\odot}/y$ , depending on the applied model and temperature profile.

We also investigate the effects of the ROSAT PSF on our estimate of  $\dot{M}$ , which tends to lead to a small overestimate of this quantity if not taken into account. This increase of  $\dot{M}$  (10-25%) can be explained by a shallower gravitational potential inferred by the broader overall profile caused by the PSF, which diminishes the efficiency of mass accretion.

We also determine the total mass of the cluster using the hydrostatic approach. At a radius of 2.1 Mpc, we estimate the total mass of the cluster ( $M_{tot}$ ) to be  $9.2 \pm 2.7 \times 10^{14} M_{\odot}$ . For the gas to total mass ratio we get  $M_{gas}/M_{tot}=0.17-0.31$ , in very good agreement with the results for other clusters of galaxies, giving strong evidence for a low density universe.

*Subject headings:* galaxies: clusters: general, individual (3C 295) and cooling flows — X-rays: galaxies — cosmology: dark matter and observations

## 1. Introduction

In recent years the investigation of distant clusters of galaxies became a key issue for the study of cosmological parameters as well as for structure formation. In addition, the comparison of the physical properties of distant with nearby galaxy clusters can give useful insight into their evolution. The distant cluster 3C 295, also known as Cl 1409+526 has been extensively studied in optical wavelength bands: Dressler & Gunn (1992) determined its velocity dispersion to be  $\sigma = 1300$  km/sec in a study of seven distant clusters of galaxies. Thimm et al. (1994) in the search for line emission in galaxies observed the cluster with an imaging Fabry-Perot interferometer and found the percentage of emission line galaxies in 3C 295 to be  $40 \pm 11\%$ . Smail et al. (1997) presented the results of a weak lensing analysis of 12 distant

clusters, among them 3C 295. The analysis they present is based on data of the *Hubble Space Telescope*. Henry & Henriksen (1986) presented the analysis of *Einstein* data of the cluster. The authors conclude that there is strong evidence for 3C 295 to host a cooling flow in the center.

Cooling flows generally occur in clusters in which the cooling time of the hot gas, the intracluster medium (hereafter ICM), is less than the age of the cluster, so that the energy loss due to radiation cannot be neglected and mechanisms for the compensation must occur. This was first found by Cowie & Binney (1977), Fabian & Nulsen (1977), and Mathews & Bregman (1978), based on the findings of observations by Uhuru (Lea et al. 1973) – for reviews see Fabian et al. (1984, 1991) and Sarazin (1986, 1988).

In recent years a handful of other high redshift clusters also show indications of hosting cooling flows in their centers. Most recently Schindler et al. (1997) reported on RXJ1347-1145 ( $z=0.45$ ) having an extremely massive cooling flow with a mass accretion rate exceeding  $3000 M_{\odot}/y$ . Fabian & Crawford (1995) reported on the detection of a cooling flow in IRAS P09104+4109 ( $z=0.442$ ) with a mass accretion rates of about  $1000 M_{\odot}/y$ , and Edge et al. (1994) found in Zwicky 3146 at  $z=0.29$  a cooling flow with similar strength.

In this paper we aim to give more insight into the cooling flow and its dependence on the temperature structure of the ICM, the gas and dark matter distribution and the overall dynamical state of 3C 295. The outline is therefore as follows: Sec.2 gives a brief description of the observation and data handling. In Sec.3 we describe our spatial analysis based on the isothermal  $\beta$ -model, which is followed by a section describing our way of calculating the X-ray luminosity of the cluster. The cooling flow analysis is presented in Sec.5. Sec.6 describes the details of our employed mass analysis. Discussion and conclusion follow hereafter.

Throughout the paper we assume  $H_0 = 50\text{km/sec/Mpc}$ ,  $q_0 = 0.5$ , and  $\Lambda = 0$ .

## 2. X-ray observations

3C 295 was observed with the ROSAT HRI for 29.6 ksec. Fig.1 shows the resulting image of the cluster. We only use channels 2 to 9 out of the 15 channels of the instrument to optimize the signal to background ratio as the neglected channels mostly have low or negligible sensitivity (for details see David et al. 1997). With about 830 source photons within a radius of 8.3 arcmin we obtain a countrate  $0.028 \pm 0.001\text{s}^{-1}$  for the cluster.

## 3. Spatial analysis

### 3.1. Overall morphology

The cluster is elongated in North-South direction with an axial ratio of 0.78 (see below and Tab.2). The emission is centrally peaked, which is a strong indication for the existence of a cooling flow (see below). There is some isophot twist visible in the contours in Fig.1. The lines are more compressed in the South-East and more stretched in the North-West. We will discuss this feature and its significance later on in more detail.

There are no other clearly extended sources visible in the vicinity of the cluster as all other emission peaks in Fig.1, which have at least two contour lines, are consistent with point sources – we checked whether these sources were possibly extended by determining their individual surface brightness profiles and comparing them to the on-axis point spread function of the ROSAT HRI.

### 3.2. Surface brightness and isothermal $\beta$ -model

The radial surface brightness profile of the cluster can be seen in Fig.2. To explore physical quantities of 3C 295 we make use of the isothermal  $\beta$ -model (Cavaliere & Fusco-Femiano 1976, 1981; Sarazin 1986). This model enables us to convert the brightness profile of a cluster analytically into a density profile of the gas. The one-dimensional surface brightness profile of this model has the following form:

$$S(r) = S_0 \left(1 + \frac{r^2}{a^2}\right)^{-3\beta+1/2} + B, \quad (1)$$

which translates into a density profile:

$$n(r) = n_0 \left(1 + \frac{r^2}{a^2}\right)^{-3\beta/2}, \quad (2)$$

where  $a$  (the so-called core radius),  $S_0$  (the central surface brightness),  $B$  (the background) and  $\beta$  are all fit parameters.

There exists also a two-dimensional form of the isothermal  $\beta$ -model which takes into account a possible elongation of the cluster. This model has the representation :

$$S(x, y) = S_0 (1 + F_1 + F_2)^{-3\beta+1/2} + B; \quad (3)$$

$$\text{with: } F_1 = \frac{(\cos(\alpha)(x - x_0) + \sin(\alpha)(y - y_0))^2}{a_1^2}; F_2 = \frac{(-\sin(\alpha)(x - x_0) + \cos(\alpha)(y - y_0))^2}{a_2^2}.$$

We apply in the following the one-dimensional and the two-dimensional isothermal  $\beta$ -model to the data. The first model has four fit parameters ( $S_0$ ,  $a$ ,  $\beta$ ,  $B$ ), the second eight fit parameters ( $S_0$ ,  $a_1$ ,  $a_2$  - two core radii, one for the major axis, one for the minor axis,  $\beta$ ,  $B$ ,  $x_0$ ,  $y_0$  - the position of the center of the cluster in x and y, and the position angle  $\alpha$ ). In the one-dimensional fit we predefine the center of the cluster by sorting the photons into concentric annuli centered on the peak of the X-ray cluster emission. In the two-dimensional case, where we look at pixels instead of annuli, this predefinition is not necessary and the center of the cluster emission is simultaneously fitted together with the other parameters.

The two-dimensional fit we apply here takes into account the effects of the PSF of the ROSAT HRI by convolving each tested model with the PSF before fitting. For the fitting we exclude serendipitous sources, which are clearly not connected to the X-ray emission of the cluster. The positions of these excluded sources can be seen in Tab.1.

#### 3.2.1. The one-dimensional fit

For the one-dimensional fit we bin the data in concentric annuli with a width of 10 arcsec. The results for this fit give a core radius of  $a = 7.2_{-3.3}^{+3.4''} \equiv 50_{-23}^{+23}$  kpc and a slope parameter of  $\beta = 0.56_{-0.07}^{+0.10}$  (2  $\sigma$ -errors). The reduced  $\chi^2$  of the fit is 1.03, which gives a very high confidence in the fit results. The fitted profile can be seen in Fig.2, and details of the other fit parameters are given in Tab.2. Reducing the width of the annuli, in order to better resolve the central part does not significantly change the fit parameters and the connected uncertainties.

The derived quantities are in good agreement with the results obtained by Henry & Henriksen (1986), who analyzed Einstein data and derived a core radius of  $a = 9_{-4}^{+10''}$  and a  $\beta = 0.58_{-0.08}^{+0.25}$  (1  $\sigma$ -errors).

### 3.2.2. The two-dimensional fit

For the two-dimensional fit we use an image with a pixel size of  $3'' \times 3''$ , taking into account all pixels located within a radius of 2.5 arcmin from the pointing position at RA=14<sup>h</sup>11<sup>m</sup>21.6<sup>s</sup>, Dec.=52<sup>d</sup>12<sup>m</sup>00.0<sup>2</sup> (J2000).

Our fitting procedures for both the one-dimensional and the two-dimensional case are based on  $\chi^2$ -statistics. This is ideal for the one-dimensional case, in which we look at concentric annuli centered on the emission peak of the cluster, as there are always enough counts per bin to assure that the Poisson distribution in each bin is similar to a Gaussian distribution, which is required for  $\chi^2$ -fitting. The decrease in cluster emission outwards in this case is compensated by the increase in area of the annuli. However, in the two-dimensional case, in which we use image pixels all of the same size, this compensation does not occur. Here the counts per pixel, especially in outer regions, are too low to show Gaussian behaviour, but instead, show a classical Poisson distribution. To overcome the problem here, we apply a small Gaussian filter ( $\sigma = 3''$ ) to the image before fitting. This Gaussian filter changes the Poisson statistics into a Gaussian shape. For the error determination in each pixel we can fully account for the Gaussian filtering by adding the corresponding errors of all contributing pixels quadratically (the exact formalism of the error determination can be found in Neumann & Böhringer (1997)). In this way we change the errors in countrate per pixel without reducing the number of degrees of freedom. We do not lower the number of degrees of freedom here, as we would in the case of increasing the pixel size of the used image, since we keep all the available spatial information.

To account for the Gaussian filtering, which causes the inferred profile of the cluster to become shallower, we also apply the same Gaussian filter to the point spread function image with which we convolve the fitted cluster model. To prove that with this procedure we indeed are able to determine the precise shape of the cluster we constructed a simulated cluster image with known properties, similar to 3C 295, and with an equal exposure time as our analyzed ROSAT HRI pointing. We apply Poisson noise on this image and convolve it with the on-axis PSF of the ROSAT HRI. Subsequently we apply the Gaussian filter and fit the two-dimensional  $\beta$ -model to the simulated cluster image, taking into account the (Gaussian filtered) PSF. The results can be seen in Tab.3. The intrinsic cluster model properties and the obtained fit parameters agree very well within the errors, giving clear evidence that our method indeed gives correct results.

As  $\chi^2$ -statistic does not allow an error of 0, we define the error of a pixel with value 0 to have an error of 1 (before filtering). Because of this necessary modification, we are, unfortunately, not able to give a confidence level or a reduced  $\chi^2$  value of the fitted elliptical cluster model, and therefore base our error determination on a Monte Carlo-technique (see below). Our fit results are the following: for the core radii we get  $a_1 = 4.2_{-2.3}^{+2.3''} \equiv 29_{-16}^{+16}$  kpc and  $a_2 = 3.3_{-1.8}^{+1.8''} \equiv 23_{-12}^{+12}$  kpc, for the slope parameter we get  $\beta = 0.52_{-0.07}^{+0.07}$  (2 $\sigma$ -results). The results for the other six fit parameters can be seen in Tab.2 and the profile can be seen in Fig.2. One can see that while  $\beta$  is relatively unaffected by the PSF of the ROSAT HRI the same is not true for the core radius. The core radius changes when the PSF is taken into account and drops from 7.2 arcsec to 4.2 arcsec or 3.3 arcsec, respectively. However, one should note that the errors of this parameter (which are all 2  $\sigma$  errors) show a large overlap.

The approach of fitting after the application of a Gaussian filter in the two-dimensional case has been already successfully applied to other clusters, such as Cl0016 (Neumann & Böhringer 1997) and A2218 (Neumann & Böhringer 1998).

### 3.2.3. *Error estimates for the two-dimensional fit*

For the error determination of the 2d-fit parameters we apply a Monte-Carlo method for which we construct 100 artificial images by adding random Poisson noise on the real cluster image and fitting each individual Poisson image in the same way as the original image. For the errors we use two times the standard deviation of each fit parameter from the 100 different fit results.

### 3.2.4. *Comparison of the fits*

The comparison of the two fits to the original data, the one taking into account the effects of the PSF the other one not, can be seen in Fig.2. In fact, apart from the central region, which has a more peaked emission when taking into account the PSF, the differences in the surface brightness profile are rather small. Therefore we conclude that the PSF might affect the cooling flow analysis (see below), but not the overall cluster properties at large radii. In order to see whether the difference in the fit results are partly due to ellipticity, we perform a one-dimensional fit, which takes into account the effects of the PSF. The results are identical to our fit result of the two-dimensional fit, showing that the differences are only due to PSF effects.

### 3.2.5. *Effects of blurring*

In the above analysis we neglected possible errors in the aspect resolution of the instrument. In order to see whether the PSF is degraded because of effects concerning the wobbling of the telescope or the reacquisition of guide stars we compared the theoretical PSF of the telescope and HRI with point sources in the field-of-view. The comparison of theoretical and actual PSF gives somewhat different results, depending on the binning of the actual observed point sources - This effect is most likely due to Poisson noise as all point sources are with a count rate well below 0.003 cts/sec very faint. - The brightest source has about 60 source counts (see Tab.1). However, all surface brightness profiles of serendipitous sources are quite consistent with the theoretical PSF (see above). If the aspect resolution is slightly degraded, it is not possible to assess the error it introduces and it is also not possible to correct for it, due to the lack of bright sources in the pointing (for corrections concerning blurring see for example Morse 1994 and Harris et al. 1998).

This blurring can in principle effect our  $\beta$ -model fits and the resulting analysis. However, we do not expect the effects to play an important role.

## 3.3. **Search for substructure**

In order to search for possible substructure in the cluster we construct a cluster model image from the best fit parameters of our two-dimensional fit, which includes the background (the model can be seen in Fig.3). Subsequently we convolve the model with the PSF of the ROSAT HRI and subtract the model from the original data. The image of the so obtained residuals are shown in Fig.4.

In this image we find positive residuals only below a significance level of three  $\sigma$  above background and cluster emission, so that there is no strong evidence for a perturbation in the cluster potential, like a subgroup falling onto the cluster. There is a decrement in the residual map in the South-East of the cluster,

which could in principle be an indication of some disturbance. However, it could also be just an indication of a region with higher intrinsic galactic absorption. Unfortunately, surveys of the 21-cm line do not (yet) provide the necessary spatial resolution to confirm or rule out a strong gradient in galactic absorption in the line-of-sight of the cluster.

The fact that this is the only evidence that the cluster deviates from the applied cluster model weakens the case for a perturbation in the potential. To see whether this decrement might be due to an offset between the true cluster center and cluster model (which is very unlikely as the peak of emission in Fig.1 and the cluster center in Fig.3 coincide very well), we shift the center of the subtracted cluster model several arcseconds in the direction NW of the center. The decrement remains after the shift, indicating that this deficit in emission might indeed be real.

Finally, we conclude that, apart from this decrement, there is no further evidence for the cluster being dynamically young. It does not seem that the cluster is suffering or has recently suffered from a major merger phase, which is in agreement with the cluster hosting a cooling flow – normally a strong indication for a relaxed cluster. This fact is strengthened by the high confidence level of the one-dimensional fit, which one does not expect in case of a non-relaxed cluster. However, we want to stress that our 3C 295 exposure has limited signal-to-noise, and that future X-ray telescopes, such as AXAF or XMM will give further information due to higher sensitivity and lower background.

### 3.4. Central electron density

To calculate the central electron density of the cluster we employ the results of the isothermal  $\beta$ -model. Using the one-dimensional model as input we calculate a central electron density of  $n_{e0} = 0.040^{+0.007}_{-0.005} \text{ cm}^{-3}$ . For the two-dimensional  $\beta$ -model we use as mean core radius the geometrical mean of  $a_1$  and  $a_2$ , giving  $\bar{a} = 3.7''$ . The derived  $n_{e0}$  in this case is  $n_{e0} = 0.084^{+0.074}_{-0.049} \text{ cm}^{-3}$ . The errors are hardly dependent on the temperature due to the ROSAT energy band (see for example Jones & Forman 1992; Böhringer 1994) but are dependent on the intrinsic shape parameters of the isothermal  $\beta$ -model. The errors are larger for the two-dimensional case, as we take into account the errors of the two core radii, the  $\beta$  and the  $S_0$ , while for the 1-d case we only take into account the error of the one core radius and  $\beta$ .

### 4. X-ray luminosity

The ROSAT/HRI source countrate of 3C 295 is  $0.028 \pm 0.001 \text{ sec}^{-1}$ . To determine this countrate we subtract from the original data the background rate determined from the spherical symmetric  $\beta$ -model fit and exclude serendipitous sources not belonging to the cluster.

Assuming that the cluster temperature lies between  $kT = 7.1^{+2.1}_{-1.3} \text{ keV}$ , the result by Mushotzky & Scharf (1997) based on ASCA data, we obtain an X-ray rest frame luminosity of  $L_x(0.1 - 2.4 \text{ keV}) = 1.01^{+0.05}_{-0.05} \times 10^{45} \text{ erg/sec}$  in the ROSAT band, corresponding to a bolometric luminosity of  $L_x(bol) = 2.6^{+0.4}_{-0.2} \times 10^{45} \text{ erg/sec}$ . The error on the luminosity is a combination of both countrate statistics and the uncertainty in temperature. For the model we use thermal Bremsstrahlung, and a galactic hydrogen column density of  $n_H = 1.34 \times 10^{20} \text{ cm}^{-2}$  from 21cm-line measurements (Dickey & Lockman 1990). Our estimate for  $L_x(bol)$  is in reasonably good agreement with the result of Mushotzky & Scharf (1997), who obtain an X-ray luminosity of  $L_x(bol) = 1.9 \times 10^{45} \text{ erg/sec}$ , when transformed to  $g_0 = 0.5$ . The discrepancy in the luminosity estimate can have several sources. First of all the presence of colder gas in the cooling flow region might lower the effective temperature in the ROSAT band, which

is softer than the ASCA band. Secondly, the discrepancy in the luminosity estimates might be due to the large PSF of the ASCA instruments, leading normally to an underestimate of the countrate.

Our results are also in agreement with the results of Lea & Henry (1988), who determined an X-ray luminosity of  $L_x(0.5 - 4.5\text{keV}) = 9_{-0.7}^{+0.7} \times 10^{44}\text{erg/sec}$  on the basis of Einstein data.

## 5. Cooling flow analysis

### 5.1. Cooling time and cooling flow radius

In central parts of clusters of galaxies the time in which the ICM cools from several  $10^7 - 10^8\text{K}$  to temperatures several orders of magnitude less can be lower than the age of the cluster. In these regions the energy loss due to radiation is therefore not negligible and mechanisms for the compensation must occur (for details see for example Fabian et al. 1991). To give an estimate out to what radius the energy loss is not negligible one often makes use of the so-called cooling time  $t_{cool}$ , which is defined as the enthalpy of the ICM divided by the energy loss due to radiation in X-rays, *i.e.*

$$t_{cool} = \frac{\frac{5}{2}nk_bT}{n_en_h\Lambda(T)}. \quad (4)$$

Here,  $\Lambda$  is defined as cooling rate and is only dependent on metallicity and temperature. Typical values for  $\Lambda$  are in the range of  $1 - 3 \times 10^{-23}\text{erg s}^{-1}\text{cm}^6$ . Inserting our results from the isothermal  $\beta$ -model together with some estimates on  $\Lambda$  from Böhringer & Hensler (1989) (see also Tab.4), we can calculate the cooling time as function of radius. The cooling flow radius is then defined as the radius at which the cooling time is equal the cluster formation time, which depends on cosmological parameters. Assuming the cooling time to be  $t_{cool} = 7.4 \times 10^9\text{yr}$ , which corresponds to the age of the cluster at a redshift of  $z=0.46$ , we get cooling flow radii corresponding to 60–100 kpc, depending on the  $\beta$ -model and on the temperature we apply. For a comparison with nearby clusters, if we neglect the fact that we see the cluster in a younger stage than nearby ones, and assume a cooling time of  $t_{cool} = 10^{10}$  y, we get cooling flow radii in the range of 70–120 kpc.

### 5.2. Mass accretion rates

If we assume that the only efficient mechanisms which compensate the energy loss due to radiation in the center of the cluster are mass accretion and cooling of the ICM, we can write for the energy balance

$$n_e(r)n_h(r)\Lambda(T) = \frac{\dot{M}(r)}{4\pi r^2} \left( \frac{5k}{2\mu m_p} \frac{dT}{dr} + \frac{d\Phi(r)}{dr} \right), \quad (5)$$

where  $\Phi$  is the gravitational potential. The left hand side of this equation is the energy loss due to radiation as function of radius, the right hand side shows the mechanisms of compensation: cooling and accretion. Now, we can insert our results of the isothermal  $\beta$ -model in equ(5) and calculate the mass accretion. To determine the gravitational potential we can use the hydrostatic equation

$$\frac{dP}{dr} = -\rho_{gas} \frac{d\Phi}{dr}. \quad (6)$$

Assuming that the ICM has the same properties as an ideal gas we can, in combination with the isothermal  $\beta$ -model, calculate the gravitational potential of the cluster and with it its total mass as function of radius,

*i.e.*

$$\Phi(r) = \frac{GM(r)}{r} = -\frac{rk_bT}{\mu m_p} \left( \frac{1}{n} \frac{dn}{dr} + \frac{1}{T} \frac{dT}{dr} \right), \quad (7)$$

where  $M(r)$  is the total mass within radius  $r$ . We employ the isothermal  $\beta$ -model for the gas density distribution even though the cluster might not be isothermal as the emission in the ROSAT energy band (0.1-2.4 keV) depends only weakly on the temperature of the ICM (see above). We would like to stress here that we use the isothermal  $\beta$ -model only as fit function to deproject the surface brightness profile into a density profile of the ICM and that possible temperature gradients or the presence of multiphase gas can be neglected as the measured count rate in the ROSAT band hardly depends on cluster temperature. The use of any other analytical function instead of the  $\beta$ -model for deprojecting would not increase the reliability of the calculated density profile, as we do not have any information on the temperature distribution. Deprojecting numerically by subtracting shell by shell, as is done for nearby clusters cannot be undertaken here, as our data have too poor statistics.

We also want to note that our analysis presented here describes and assumes idealized circumstances, for example that either the cooling flow region is isothermal or has a constant temperature gradient.

### 5.2.1. The isothermal case

Assuming for now the strongly idealized case that the cluster is isothermal, and inserting equ(2), equ(6) and equ(7) in equ(5), we can directly calculate the mass accretion rate from

$$\dot{M} = \frac{4\pi\mu m_p a^2}{3k_b T \beta} n_{e0} n_{h0} \Lambda(T) r \left( 1 + \frac{r^2}{a^2} \right)^{-3\beta+1}. \quad (8)$$

With this equation one can see the dependence of  $\dot{M}$  on  $r$ ,  $a$ , and  $\beta$ . In case that the cooling flow radius is smaller than the core radius  $a$ , or in case that the  $\beta$  value is very small ( $\beta \leq 0.33$ ), the mass accretion rate is proportional to  $r$ , since then the term  $\left( 1 + \frac{r^2}{a^2} \right)^{-3\beta+1}$  almost stays constant. This is in agreement with the findings of other authors, e.g. Thomas et al. (1987), and Fabian et al. (1991), Neumann & Böhringer (1995). However, as in the case of 3C295 the core radius is between 25 kpc and 50 kpc and therefore smaller than the cooling flow radius, and as  $\beta \geq 0.33$ , the term  $\left( 1 + \frac{r^2}{a^2} \right)^{-3\beta+1}$  changes significantly and therefore influences the shape of the mass accretion rate as a function of radius. The results can be seen in Fig.5 (for the isothermal  $\beta$ -model taking into account the PSF) and Fig.6 (for the isothermal  $\beta$ -model neglecting the effects of the PSF). The maximal mass accretion rate is in the range 550–900  $M_\odot/y$ , depending on the assumed temperature. In the isothermal case the mass accretion rates rise with radius up to 50 kpc and then stay more or less constant.

### 5.2.2. The case of constant temperature gradient

It is generally found that the temperatures in cooling flow regions are lower than the overall cluster temperature. Often a temperature gradient in the cooling flow region can be observed. If we assume that there exists a constant temperature gradient in the cooling flow region of 3C 295, we can rewrite equ(5) as

$$\dot{M} = \frac{4\pi r^2 \mu m_p n_{e0} n_{h0}}{3k_b} \frac{\left( 1 + \frac{r^2}{a^2} \right)^{-3\beta} \Lambda(T)}{\frac{r(\text{grad}_T r + T_{\text{center}})\beta}{a^2 \left( 1 + \frac{r^2}{a^2} \right)} + \frac{\text{grad}_T}{2}}, \quad (9)$$

where  $grad_T$  is the temperature gradient one infers and  $T_{center}$  is the central temperature. In equ(9) we take into account that a temperature gradient changes the shape of the gravitational potential (see equ(7)). We assume that the gas is still in hydrostatic equilibrium and that the hydrostatic equation equ(7) is still applicable, assuming a single phase ICM. One way to see this: while the gas is cooling down its density distribution changes accordingly to fulfill equ(7). For our calculation of mass accretion rates we assume the temperature at the center to be 2 keV and at a radius of 120 kpc to be either 5.8, 7.1, or 9.2 keV – the range of temperatures representing the error in the determination of the overall temperature of 3C 295 by Mushotzky & Scharf (1997). For simplification we assume that  $\Lambda(T)$  is linear in temperature between 2 to 10 keV. The adopted values for  $\Lambda$  can be seen in Tab.4. For intermediate temperatures we interpolate linearly. The results of our calculations are shown in Fig.5, and Fig.6, respectively. Applying a temperature gradient lowers the mass accretion rates and changes the shape of the mass accretion rate as a function of radius. The maximum mass accretion rate occurs close to the core radius of either model, being in the range of 400–600  $M_{\odot}/y$ . After its maximum the mass accretion rate drops at larger radii – the mass accretion rate at 120 kpc varies between 300–500  $M_{\odot}/y$ .

### 5.3. Comparison with previous work

Already Henry & Henriksen (1986) analyzing Einstein IPC and HRI data suggested that 3C 295 hosts a cooling flow in the center. The authors calculated a mass accretion rate ( $\dot{M}$ ) of about 145  $M_{\odot}/y$ . The determination of  $\dot{M}$  was based on pointlike excess emission over the best fit isothermal  $\beta$ -model in the center. As one can see in Fig.2, we do not see excess emission in the center. The isothermal  $\beta$ -model coincides very well with the cluster emission in the center. This suggests two possibilities: the first one being that there was an active point source in the center of the cluster, while it was exposed with the Einstein HRI, and this source was not anymore active when exposed with the ROSAT HRI. The second possibility is that because Henry & Henriksen (1986) simultaneously fitted a point source and an isothermal  $\beta$ -model to the data, this led to an overestimate of the central point source resulting from an underestimate of the emission from the cluster itself. A weak indication for this is the fact that Henry & Henriksen obtain a core radius of  $a = 9_{-4}^{+10''}$  and a  $\beta = 0.58_{-0.08}^{+0.25}$  – both values being higher than our best fit results. However, the overall agreement between Einstein and ROSAT data is very encouraging. The higher fit values for core radius and  $\beta$  obtained by Henry & Henriksen (1986) cause the estimated cluster profile to be flatter in the center than in our fitted models.

### 5.4. Contamination by radio or point sources emitting in X-rays

The cluster of galaxies 3C 295 is known to host a luminous radio source in the center (Akujor et al. 1994 and references therein). The source consists of two radio lobes with a separation of about 5 arcsec. The extent of the lobes is each about 2 arcsec. In principle the spatial resolution of the HRI is sufficient to resolve these lobes, if they emit in X-rays. However the Poisson statistics, which is the factor which really limitats the spatial resolution here, makes a detection of their separation difficult. It is also not clear whether these lobes lead to an enhancement in X-rays or diminish the X-ray brightness in this area. An example of radio lobes dimming the X-ray luminosity in the center of a cluster was shown by Böhringer et al. (1993) for the Perseus cluster or Schindler & Prieto (1997) in the case of A2634. Strong evidence that these sources are not very prominent and do not obscure the X-ray surface brightness

profile is the fact that we yield a very high confidence level for the isothermal  $\beta$ -fit with a reduced  $\chi^2=1.03$ . The good agreement between fit and real data is difficult to explain in the presence of additional sources in the center, whether they enhance or diminish the X-ray brightness, as they affect the overall fit.

Also a single point source in the center can be ruled out by the same argument. It seems very unlikely that a central point source would have exactly the “right” emission to fit the model. Also, in this unlikely scenario, a central source would affect the profile only out to about 3–5 arcsec – the size of the PSF. As our calculated cooling flow radius is larger than this (12'' – 17''), a single central point source cannot explain the X-ray peak in the center.

Another test to see whether a central point source can influence the surface brightness profile in the center of the cluster is to perform an isothermal  $\beta$ -model fit (one-dimensional) neglecting the innermost bin of the radial profile (see Fig.2). This central bin should contain almost all emission from a central point source, if present. The result of this fit leads to an even more centrally peaked cluster model, with a best fit result for the core radius of about 1.5 arcsec, a  $\beta = 0.54$  and a very high central surface brightness of  $S_0 = 8.3 \times 10^{-4} \text{sec}^{-1} \text{arcsec}^{-2}$ . However, this fitted model has much larger error bars than the original one-dimensional fit, and the uncertainties in core radius and  $\beta$  of the original fit are very well encompassed in the error estimates of the modified fit.

Putting this all together, we conclude that if there are other individual X-ray sources present in the center of the cluster, then their effect on the cooling flow analysis is negligible, and they are unlikely to lead to a dramatic overestimate of the mass accretion rates.

## 6. Mass analysis

To determine the total and the gas mass of the cluster we utilize the results of the isothermal  $\beta$ -model fitting for the gas density profile. We assume that the temperature throughout the whole cluster lies between 5.8-9.2 keV, which are the results obtained by Mushotzky & Scharf (1997) analyzing ASCA data. For the mass determination we assume spherical symmetry and hydrostatic equilibrium and under these assumptions we can use equ(7). These assumptions are justified and lead to reliable estimates for the mass determination of clusters of galaxies as shown by Schindler (1996) and Evrard et al. (1996), who analyzed hydrodynamic simulations under these assumptions and compared the obtained results with the intrinsic properties. For the determination of the total mass we perform a Monte-Carlo analysis (Neumann & Böhringer 1995), which calculates possible random temperature variations within the above given limits. For the stepwidth of these temperature variations we use 300 kpc. As the uncertainties in temperature by far exceed the uncertainties in the density profile we neglect here the errors of the isothermal  $\beta$ -model, which introduce errors in the density distribution of the gas.

As a smoothing parameter, to avoid strong and unphysical oscillations of the temperature profiles, we use  $\Delta T = 0.3$  keV, which means that each temperature at a certain radius has to lie within 0.3 keV of the adjacent step radius. the temperature of the next inner step radius  $T \pm 0.3$  keV. The results can be seen in Fig.7 and Tab.5. Calculating the total mass of the cluster we get  $M_{tot} = 9.2 \pm 2.7 \times 10^{14} M_{\odot}$  at a radius of 2.1 Mpc. The result is slightly dependent on the employed  $\beta$ -model. For the gas to total mass ratio we get  $M_{gas}/M_{tot} = 0.18^{+0.08}_{-0.04}$  for  $\beta = 0.56$  and  $M_{gas}/M_{tot} = 0.22^{+0.09}_{-0.05}$  for  $\beta = 0.52$ . A summary of the results is given in Tab.5.

## 7. Discussion

### 7.1. Cooling flow and $\beta$ -model fitting

Despite the fact that 3C 295 hosts a cooling flow, we do not see evidence for central excess emission above the fitted isothermal  $\beta$ -model as seen in almost all other cooling flow clusters. Normally, fitting an isothermal  $\beta$ -model to the X-ray data of these kind of clusters leads to results which underestimate the central emission. However, most of these studies are based on nearby clusters, which can be traced out to larger radii than 3C 295. We can trace the X-ray emission of 3C 295 only out to a radius of 2.0-2.5 arcmin (see Fig.2), which corresponds to 900-1100 kpc. Therefore we are unable to see the outer parts of the cluster and our fit is only based on the central parts. Fits of this kind, where one only takes into account the center of a cooling flow cluster, generally lead to smaller core radii and  $\beta$ 's. Our values for core radius and  $\beta$  are also relatively small, when compared to other clusters, which generally have core radii ranging between several 100 kpc and  $\beta$ 's, which lie between 0.6 and 0.9 for rich and X-ray luminous clusters of galaxies. Therefore we conclude that the reason we do not see a central excess lies solely in the fact that we see and fit only the central part of 3C 295. For an analogy, we more or less see only the tip of the iceberg. Future X-ray instruments such as aboard on AXAF or XMM, which have higher sensitivity and lower background than the ROSAT/HRI will enable us to trace distant clusters out to much larger radii.

### 7.2. The effects of the PSF on the cooling flow analysis

We determine two different isothermal  $\beta$ -models in our spatial analysis: one takes into account the effects of the PSF and ellipticity, and gives a  $\beta = 0.52$  and a small core radius ( $\bar{a} = 3.7$  arcsec), while in the other one neglects PSF effects which gives  $\beta = 0.56$  with a larger value for the core radius ( $a = 7.2$  arcsec). Comparing the results of the subsequent cooling flow analysis of the two models, one can see that in the  $\beta = 0.56$  case we overestimate the cooling flow radius and the mass accretion rates (see Fig.5 and Fig.6). The reason why we determine a larger cooling flow radius when using the  $\beta = 0.56$  model instead of the  $\beta = 0.52$  model lies in the fact that the inferred gas density profile shows a less steep drop in the first case. This comes from the fact that the PSF makes the appearance of the profiles more shallow. Even though the calculated central electron density is lower in the  $\beta = 0.56$  case, the densities of the gas are equal in both models at a radius of 60 kpc, and at larger radii the  $\beta = 0.56$  model gives higher values for the gas density than the  $\beta = 0.52$  case. The consequence is that the cooling times in the  $\beta = 0.56$  case at radii larger than 60 kpc are smaller than the ones of the other model, due to the fact that  $t_{cool} \propto n^{-2}$ . As the cooling flow region is determined by its cooling time being less than a certain time interval, the cooling flow radius is, of course, bigger in the  $\beta = 0.56$  case. The overestimate of the cooling flow radius is of the order of 20%, but does not have a big influence on the resulting maximal mass accretion rate, as at outer regions the mass accretion rate stays almost constant. The overestimate of the mass accretion rates in the  $\beta = 0.56$  case again results from a shallower profile, in this case from the gravitational potential. A shallower potential stands for a smaller potential gradient and this means that more gas must flow into the center to compensate the energy loss due to radiation (see equ(5)). The overestimate of the mass accretion rate due to PSF effects is of the order of 10–25%, which is not very high given all the other uncertainties of the physical properties, which enter the determination of the mass accretion rates.

### 7.3. Mass accretion rates and temperature gradient

Introducing a temperature gradient in the center of the cluster reduces the resulting mass accretion rates (see Fig.5 and Fig.6). This shows how sensitive the determination of mass accretion rates is on the temperature structure of the ICM. With a temperature gradient the gas has another mechanism to compensate for the energy loss due to radiation (we assume here the case of a homogenous cooling flow): while the gas is falling into the center it not only loses potential energy but also kinetic energy due to cooling. However, assuming that the hydrostatic equation is valid in this region, and assuming that multiphases in the gas are negligible, a temperature gradient also causes the gravitational potential to be more shallow (see equ.(7)). Due to this shallower potential the energy supported by loss of potential energy of the gas falling inwards is not as efficient as in the isothermal case. However, as the overall mass accretion rates drop, the effect of cooling compensates easily the effect of a shallower gravitational potential. We only want to stress here that our assumed models for the cooling flow are simple, as we, for example, neglect the presence of a multiphase gas in the cooling flow region. However, as 3C 295 is a very distant cluster, a fact which makes a more detailed analysis of the cooling flow almost impossible at the moment, we only want to give an idea of what mechanisms occur in the cooling flow region of this cluster, and how sensitive the analysis is to the observational uncertainties.

### 7.4. Correlation mass accretion rate and cooling flow radius

Comparing the determined mass accretion rate and the calculated cooling flow radius with other clusters, for example the sample of White et al. (1997), one can see that 3C 295 is relatively outstanding. It shows a very high mass accretion rate for its size of cooling flow radius. Following the fit results of White et al. (1997), the cluster should have a mass accretion rate of about  $60 M_{\odot}/y$  with a cooling flow radius of roughly 100 kpc – alternatively, with its mass accretion rate it should have a cooling flow radius of about 200 kpc. However, the difference between the calculation of White et al. and here is that we neglect inhomogeneities in the cooling flow, in which material can cool out completely and provides additional energy resources for radiation. But it is very unlikely that this effect causes the mass accretion rate to drop by a factor of ten. The discrepancy lies more likely in the fact that White et al. look at clusters at a redshift  $z < 0.2$ , while 3C 295 lies at  $z=0.46$ . It might be that the discrepancy is some sort of evolutionary effect. This idea is strengthened by another high redshift cooling flow cluster RXJ1347-1145 (Schindler et al. 1997) at  $z=0.45$  with a mass accretion rate of  $\dot{M} > 3000 M_{\odot}/y$ , and a cooling flow radius of 200 kpc, which also does not fit in the relation of White et al.. Also the results of two other distant clusters, Zwicky 3146 ( $z=0.291$ ) and Abell A1835 ( $z=0.252$ ) by Edge et al. (1994) and Allen et al. (1996a) show mass accretion rates also somewhat too large for their cooling flow radii to match the result by White et al.. It is therefore important to look at other high redshift cooling flow clusters, to see whether this is indeed an effect depending on redshift, or whether it is just that these clusters are exceptional in their properties.

### 7.5. The baryon fraction in 3C 295

The determined gas to total mass ratio in 3C 295 is  $M_{gas}/M_{tot} \sim 0.22$  – similar to the findings in other clusters. As the gas to total mass ratio is a limit on the baryon fraction in clusters, which is thought to be representative for the universe in total (based on numerical simulations, see for example Evrard 1990; Cen & Ostriker 1993), this approach can be used to measure the fraction of baryon to dark matter density in

the entire universe (the mass in galaxies in clusters is only a small fraction of the mass of the ICM). As studies of primordial nucleosynthesis give precise values of  $\Omega_b$  (the ratio of baryon to critical density of the universe), with  $\Omega_b h_{50}^2 = 0.05 \pm 0.01$  (see for example Walker et al. 1991) this can be directly used to determine  $\Omega_{tot}$ , the total density of the universe, as shown by Briel et al. (1992) and White et al. (1993) in calculating  $\frac{M_{gas}}{M_{tot}} = \frac{\Omega_b}{\Omega_{tot}} = \frac{0.05 \pm 0.01}{\Omega_{tot}}$ . The determined values of  $\Omega_{tot}$  range between 0.2–0.4, and give strong evidence for a low density universe. Our values of the gas to total mass ratio of 3C 295 suggest  $\Omega_{tot} = 0.1 - 0.4$ . The errors in the determination of  $\Omega$  come almost exclusively from the uncertainties in  $M_{tot}$ .

### 7.6. Mass estimates compared to weak lensing results

Fig.7 shows the total mass profile of 3C 295.

To be able to compare our results for the mass with the weak lensing study by Smail et al. (1997) (-the lensing approach determines the total mass along the line-of-sight within a certain radius), we also show the (along the line-of-sight) projected mass profile. We project out to a radius of 3 Mpc.

There is some discrepancy between the mass results from the lensing analysis and from the hydrostatic equation used here. The lensing result gives a higher mass. The values differ by a factor of less than two. Both estimates have relatively large error bars, which, however, do not overlap.

Where can this discrepancy come from? Partly it can be due to the fact that the mass inferred from X-rays is biased downward due to the cooling flow. The cooling flow in the central parts of the cluster could lower the measured overall temperature by ASCA due to cooled gas. Also the small values for  $\beta$  and core radius, typical for a cluster with a central cooling flow might bias the value for the inferred mass downward - the mass calculated from the hydrostatic approach is proportional to  $\beta$ . And finally the fact that we do not see the outer regions of the cluster in X-rays could systematically lower the result of our mass determination. On the other hand the mass determined with the weak lensing approach is dependent on the mean redshift of the lensed galaxies. While this is not a strong effect for nearby clusters it plays an important role for distant clusters such as 3C 295. Smail et al. (1997) used an approach with a mean redshift of the background galaxies of  $z=0.83$ . Increasing the value to for example  $z=1$  lowers the inferred mass considerably. An indication that the mass from the weak lensing might be estimated too high is the fact that the M/L for this cluster found by Smail et al.(1997) is relatively high in comparison with other clusters in their sample. Therefore it might be that the different results of the mass can be entirely explained by systematic errors in the two approaches. However, we cannot rule out that there might be some physical reason for this apparent discrepancy of the mass results, and that for example 3C 295 has either prolate symmetry along the line-of sight or suffers from projection effect from another massive structure.

## 8. Conclusions

In this paper we analyse ROSAT HRI data of the distant cluster 3C 295. We fit a one and a two-dimensional isothermal  $\beta$ -model to the data, the two-dimensional fit taking into account the ellipticity of the cluster and effects of the PSF. The one-dimensional model which does not take into account the PSF gives higher values for  $\beta$  and the core radius  $a$ ; however, the results agree within the error bars. To determine the errors of the parameters of the two-dimensional fit we use a Monte-Carlo approach. Calculating the cooling time of the central region we confirm previous findings by Henry & Henriksen (1986) of a central cooling flow. We estimate the cooling flow radius to lie between 60–120 kpc, depending on the

model and adopted cooling time for the cluster. Generally we find that the isothermal  $\beta$ -model, which does not take into account the effects of the PSF, gives higher values for the cooling flow radius and the mass accretion rates.

For the determination of the mass accretion rates we present a simple model, which is solely based on the isothermal  $\beta$ -model, neglecting heat conduction, inhomogenities and heat sources. We show that the inferred mass accretion rates, with values of  $\dot{M} = 400 - 900 M_{\odot}/y$  are dependent on the temperature structure in the cooling flow region. A temperature gradient generally lowers the mass accretion rates.

The mass accretion rate in the central part of 3C 295 is somewhat too high for its cooling radius, when compared to the sample of nearby clusters of White et al. (1997). As 3C 295 is not the only distant cluster showing this behaviour, this might be an indication that generally this relationship between mass accretion rate and cooling flow radius is evolving with time.

To search for substructure in the cluster we subtract a two-dimensional cluster model, following the best fit results of the isothermal  $\beta$ -model from the original data. Apart from a decrement in the South-East in the cluster, which might be caused by absorption, we do not find strong indication for the cluster to deviate from hydrostatic equilibrium. The fact that 3C 295 seems to be in complete hydrostatic equilibrium, and has had enough time to form a cooling flow is an indication that the cluster must have had considerably time to relax, which suggests a low density universe, with or without a cosmological constant.

Calculating the total mass of the cluster based on the hydrostatic equation using a temperature estimate of Mushotzky & Scharf (1997), we obtain results of  $M_{tot} = 9.2 \pm 3. \times 10^{14} M_{\odot}$  at a radius of 2.1 Mpc. For the gas to total mass ratio we obtain  $M_{gas}/M_{tot} \sim 0.17 - 0.31$ . This ratio is typical for other clusters, and is again a strong indication for a low density universe.

I like to thank M. Arnaud, S. Schindler and H. Böhringer for very helpful discussions, and Jean-Luc Sauvageot for computer and software support. I like to especially thank C.A. Collins for a very careful reading of the manuscript and the referee, Andy Fabian for his very useful comments. ROSAT is supported by the BMFT. I thank the CNRS and the MPG for funding.

## REFERENCES

- Akujor C.E., Lüdke E., Browne I.W.A., Leahy J.P., Garrington S.T., Jackson N., & Thomasson P 1994, A&AS, 105, 247
- Allen S.W., Fabian A.C., Edge A.C., Bautz M.W., & Furuzawa A. 1996a, MNRAS, 283, 263
- Allen S.W., Fabian A.C., & Kneib J.P. 1996b, MNRAS, 279, 615
- Böhringer H., & Hensler G. 1989, A&A, 215, 147
- Böhringer H., Voges W., Fabian A.C., Edge A.C., & Neumann D.M. 1993, MNRAS, 264L, 25
- Böhringer H. 1994, in Proceedings of the NATO Advanced Study Institute on Cosmological Aspects of X-ray Clusters of Galaxies, ed. W. Seitter (Boston: Kluwer), 123
- Böhringer H., Tanaka Y., Mushotzky R.F., Ikebe Y., & Hattori M. 1998, A&A, in press
- Briel U.G., Henry J.P., & Böhringer H. 1992, A&A, 259, L13

- Cavaliere A.,& Fusco-Femiano R. 1976, A&A 49, 137
- Cavaliere A.,& Fusco-Femiano R. 1981, A&A 100, 194
- Cen R.,& Ostriker J.P. 1993, ApJ, 417, 404
- Cowie L.L.,& Binney J. 1977, ApJ, 215, 723
- David L.P. et al. 1997, The ROSAT High Resolution Imager (HRI) Calibration Report, U.S. ROSAT SCIENCE DATA CENTER/SAO
- Dickey J.M.,& Lockman F.J. 1990, A&AR, 28, 215
- Dressler A.,& Gunn J.E., 1992, ApJS, 78, 1
- Edge A.C., Fabian A.C., Allen S.W., Crawford C.S., White D.A., Böhringer H.,& Voges W. 1994, 270, L1
- Evrard A.E., Metzler C.A.,& Navarro J.N., 1996, ApJ, 469, 494
- Evrard A.E. 1990, 363, 349
- Fabian A.C.,& Nulsen P.E.J. 1977, MNRAS, 180, 479
- Fabian A.C., Nulsen P.E.J.,& Canizares C.R. 1984, Nat. 310, 733
- Fabian A.C., Nulsen P.E.J.,& Canizares C.R. 1991, A&AR, 2 191
- Fabian A.C.,& C.S. Crawford 1995, MNRAS, 274, L63
- Harris D.E., Silverman J.D., Hasinger G., Lehmann I. 1998, A&AS, 133, 431
- Henry J.P.,& Henriksen M.J. 1986, ApJ, 301, 689
- Hewitt A.,& Burbidge G. 1991, ApJS, 75, 297
- Hewitt A.,& Burbidge G. 1993, ApJS, 87, 451
- Jones C.,& Forman W. 1992, Clusters and Sperclusters of Galaxies, ed. A.C. Fabian (Dordrecht: Kluwer), 49
- Lea S.M., Silk J., Kellog E.,& Murray S. 1973, ApJ, 184, L105
- Lea S.M.,& Henry J.P. 1988, ApJ, 332, 81
- Mathews W.G.,& Bregman J.N. 1978, ApJ, ApJ, 244, 308
- Morse J.A. 1994, PASP, 106, 675
- Mushotzky R.F.,& Scharf C.A. 1997, ApJ, 482, L13
- Neumann D.M.,& Böhringer H. 1995, A&A, 301, 865
- Neumann D.M.,& Böhringer H. 1997, MNRAS, 289, 123
- Neumann D.M.,& Böhringer H. 1998, ApJ, submitted
- Pierre M., Le Borgne J.F., Soucail G.,& Kneib J.P. 1996 A&A, 311 413

- Sarazin C. 1986, *Rev. Mod. Phys.* 58, 1
- Sarazin C. 1988, *X-ray emission from Clusters of Galaxies*, C.U.P.
- Schindler S., 1996, *A&A*, 305, 756
- Schindler S., Hattori M., Neumann D.M.,& Böhringer H. 1997, 317, 646
- Schindler S.,& Prieto M.A. 1997, *A&A*, 327, 37
- Smail I., Ellis R.S., Dressler A., Couch W.J., Oemler A.Jr., Sharples R.M.,& Butcher H. 1997, *ApJ*, 479, 70
- Squires G., Kaiser N., Babul A., Fahlman G., Woods D., Neumann D.M.,& Böhringer H. 1996, *ApJ*, 461, 572
- Squires G., Neumann D.M., Kaiser N., Arnaud M., Babul A., Böhringer H., Fahlman G.,& Woods G. 1997, *ApJ*, 482, 648
- Thimm G.J., Röser H.-J., Hippelein H.,& Meisenheimer K. 1994, *A&A*, 285, 785
- Thomas P.A., Fabian A.C.,& Nulsen P.E.J. 1987, *MNRAS*, 228, 973
- Walker T.P., Steigman G., Kang H., Schramm D.M.,& Olive K.A. 1991, *ApJ*, 376, 51
- White D.A., Jones C.,& Forman W. 1997, *MNRAS*, 292, 419
- White S.D.M., Navarro J.F., Evrard A.E.,& Frenk C.S. 1993, *Nat.* 366, 429

**Fig.1**

The countrate image of the HRI image of 3C 295. We use only channel 2 to 9 to optimize the signal to background ratio (for details see text). The image is Gaussian filtered with a  $\sigma$  of 3.5 arcsec. The contour levels are spaced logarithmically with  $\Delta = 0.26$ . The lowest contour lies at 7.22 cts/sec/arcmin<sup>2</sup>. The image is centered on R.A.=14<sup>h</sup>11<sup>m</sup>20.6<sup>s</sup> and Dec.=+52<sup>d</sup>12<sup>m</sup>10<sup>s</sup> (J.2000).

**Fig.2**

Surface brightness profile of 3C 295. The crosses show the data with 1- $\sigma$ -errors in y-direction. The full line corresponds to the best fit of the one-dimensional isothermal  $\beta$ -fit not taking into account effects of the HRI's PSF ( $\beta = 0.56$ ). The dotted line shows the results of the two-dimensional model fit correcting for the PSF (with  $\beta = 0.52$ ). For displaying we utilize here as core radius the geometrical mean of the two core radii, corresponding to 25 kpc  $\equiv$  3.7 arcsec.

**Fig.3**

The cluster model corresponding to the two-dimensional fit parameters shown in Tab.2. The lowest contour and the spacing are identical with the ones in Fig.1.

**Fig.4**

The residuals of the cluster after subtracting the isothermal  $\beta$ -model following the best fit results of the two-dimensional fit including background. The model is convolved with the PSF before subtraction. The contours show the significance of the residuals above cluster plus background emission in  $\sigma$ . The dashed line is the zero  $\sigma$ -line, negative residuals are dotted, positive residuals have a full line. The step width is 1  $\sigma$  from contour to contour. The shown significance levels take into account the applied Gaussian filter of 3.5 arcsec.

**Fig.5**

Mass accretion rates in the central part of the cluster using the model taking into account the effects of the PSF ( $\beta = 0.52$ ,  $a = \sqrt{a_1 a_2} = 3.7$  arcsec). Shown are the rates as a function of radius for the isothermal case (upper lines) and for the case of constant temperature gradient (lower lines). The dotted lines correspond to a temperature of 5.8 keV, the full line to 7.1 keV, and the dashed line to 9.2 keV. For the temperature gradient case we use a central temperature of 2 keV. In this case 5.8, 7.1, and 9.2 keV are the temperatures at a radius of 120 kpc.

**Fig.6**

The same as previous figure, only difference: we use here the isothermal  $\beta$ -model from the one-dimensional fit, not taking into account the effects of the PSF.

**Fig.7**

Mass profile of the cluster 3C 295. The full lines correspond to the  $\beta$ -model taking into account PSF effects with  $\beta = 0.52$  and a core radius of  $a = \sqrt{a_1 a_2} = 3.7$  arcsec. The dots show the result for the model with  $\beta = 0.56$ . Shown are the mean values  $\pm 2\sigma$ -errors. The open circles with the long dashed lines correspond to the projected mass profile with  $\beta = 0.52$  ( - here we only show the error limits  $\pm 2\sigma$ -errors). The dotted line shows the gas mass profile with the  $\beta = 0.52$ -model, the dashed line the profile with  $\beta = 0.56$  using a gas temperature of  $7.1_{-1.3}^{+2.1}$  keV (Mushotzky & Scharf 1997). The vertical line at 400 kpc shows the result of the weak lensing analysis by Smail et al. (1996) transformed to  $H_0 = 50$ .

Table 1: Serendipitous sources in the FOV of 3C 295

source	RA.	Dec.	total counts
1 galaxy ( $z=0.2737$ ) <sup>1</sup>	$14^h 11^m 21.5^s$	$+52^d 12^m 53^s$	10
2 galaxy ( $z=0.4733$ ) (Sy1) <sup>12</sup>	$14^h 11^m 23.1^s$	$+52^d 13^m 32^s$	60
3 QSO ( $z=1.29$ ) <sup>13</sup>	$14^h 11^m 19.2^s$	$+52^d 14^m 05^s$	20

The sources agree within 6 arcsec with the X-ray position.

<sup>1</sup> Dressler & Gunn 1992

<sup>2</sup> Hewitt & Burbidge 1991

<sup>3</sup> Hewitt & Burbidge 1993

Table 2: Isothermal  $\beta$ -fit results

	$S_0$ [ $s^{-1}\text{arcsec}^{-2}$ ]	$a_1$ [arcsec]	$a_2$ [arcsec]	$\beta$	$x_0$ 2000.0	$y_0$ 2000.0	$\alpha$	$B$ [ $s^{-1}\text{arcsec}^{-2}$ ]
1-d	$3.8 \times 10^{-5}$	$7.2^{+3.4}_{-3.3}$		$0.56^{+0.10}_{-0.07}$	$14^h 11^m 20.3^s$	$52^d 12^m 12^s$		$9.6 \times 10^{-7}$
2-d	$9.2^{+7.0}_{-7.0} \times 10^{-5}$	$4.2^{+2.3}_{-2.3}$	$3.3^{+1.8}_{-1.8}$	$0.52^{+0.07}_{-0.07}$	$14^h 11^m 20.2^s$	$52^d 12^m 12^s$	$14^{+27^\circ}_{-27^\circ}$	$9.1^{+0.09}_{-0.10} \times 10^{-7}$

Table 3: Fit results of the simulated cluster model

	$S_0$ [ $s^{-1}\text{arcsec}^{-2}$ ]	$a_1$ [arcsec]	$a_2$ [arcsec]	$\beta$	$x_0$ [arcsec]	$y_0$ [arcsec]	$\alpha$	$B$ [ $s^{-1}\text{arcsec}^{-2}$ ]
input	$9.2 \times 10^{-5}$	4.2	3.3	0.52	0.0	0.0	$14^\circ$	$9.0 \times 10^{-7}$
fit	$10.5^{+5.8}_{-5.8} \times 10^{-5}$	$4.0^{+2.0}_{-2.0}$	$3.2^{+1.5}_{-1.5}$	$0.52^{+0.05}_{-0.05}$	$0.0^{+0.7}_{-0.7}$	$0.0^{+0.8}_{-0.8}$	$14^{+28^\circ}_{-28^\circ}$	$9.1^{+0.7}_{-0.7} \times 10^{-7}$

Table 4: Cooling rates - adopted from Böhringer & Hensler (1989).

$\Lambda(T)$ [ $10^{-23}\text{erg s}^{-1} \text{cm}^6$ ]	$k_b T$ [keV]
1.4	2.0
2.1	5.8
2.3	7.8
2.6	9.2

Table 5: Results of the Monte Carlo mass analysis

	total mass ( $\beta = 0.52$ ) [ $10^{14}M_\odot$ ]	total mass ( $\beta = 0.56$ ) [ $10^{14}M_\odot$ ]	gas mass ( $\beta = 0.52$ ) [ $10^{14}M_\odot$ ]	gas mass ( $\beta = 0.56$ ) [ $10^{14}M_\odot$ ]
at 2.1 Mpc	$9.2 \pm 2.7$	$9.9 \pm 3.0$	2.0	1.8

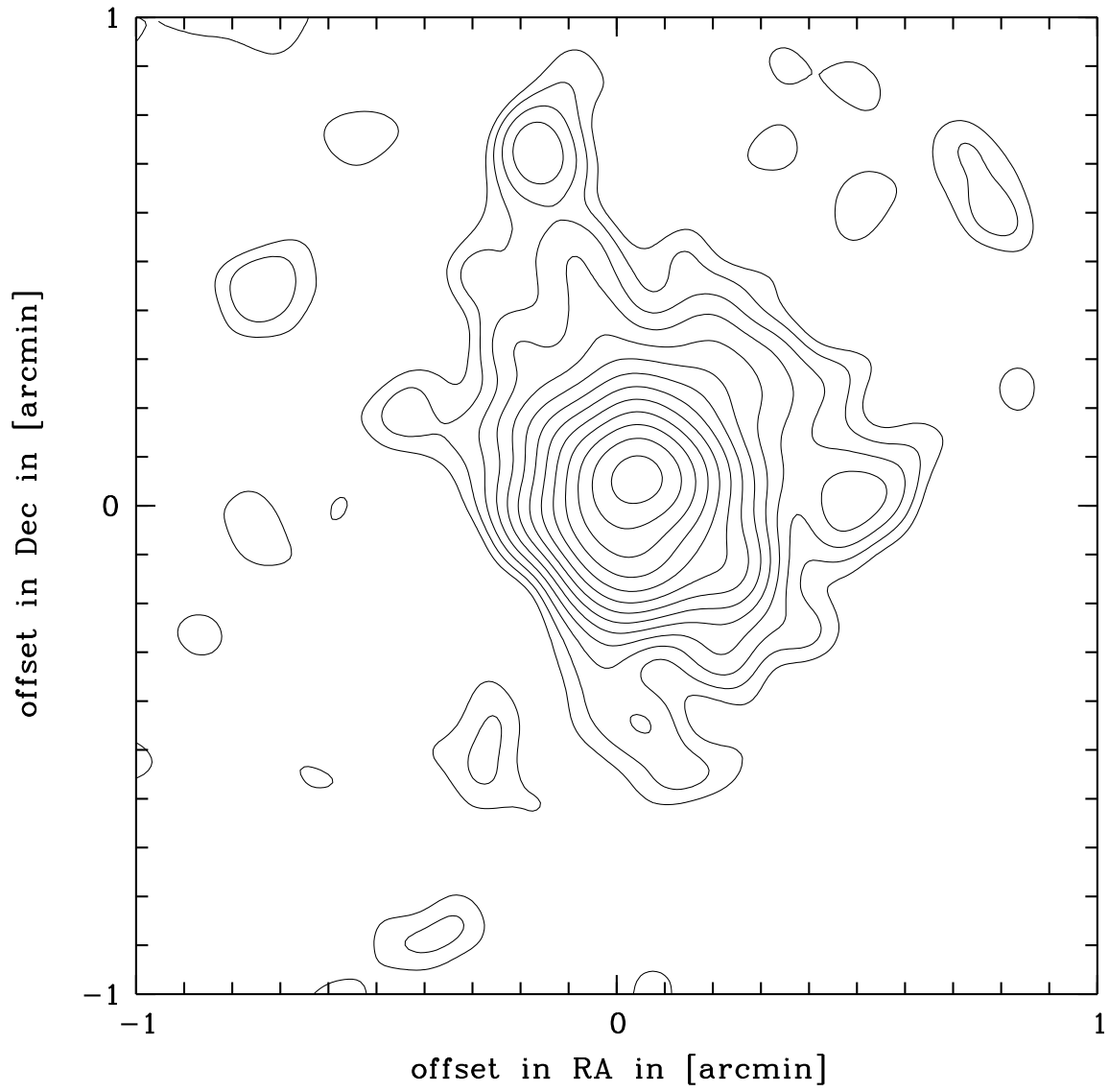


Fig. 1.—

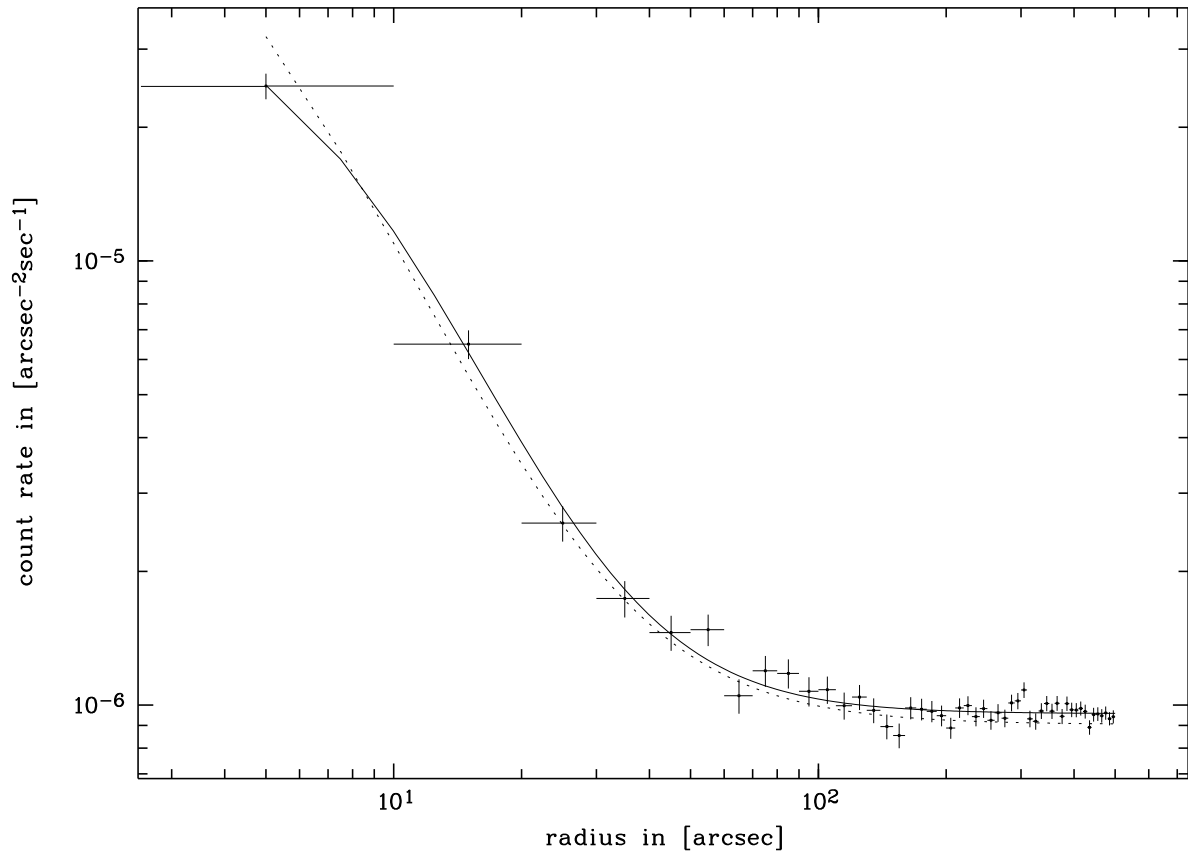


Fig. 2.—

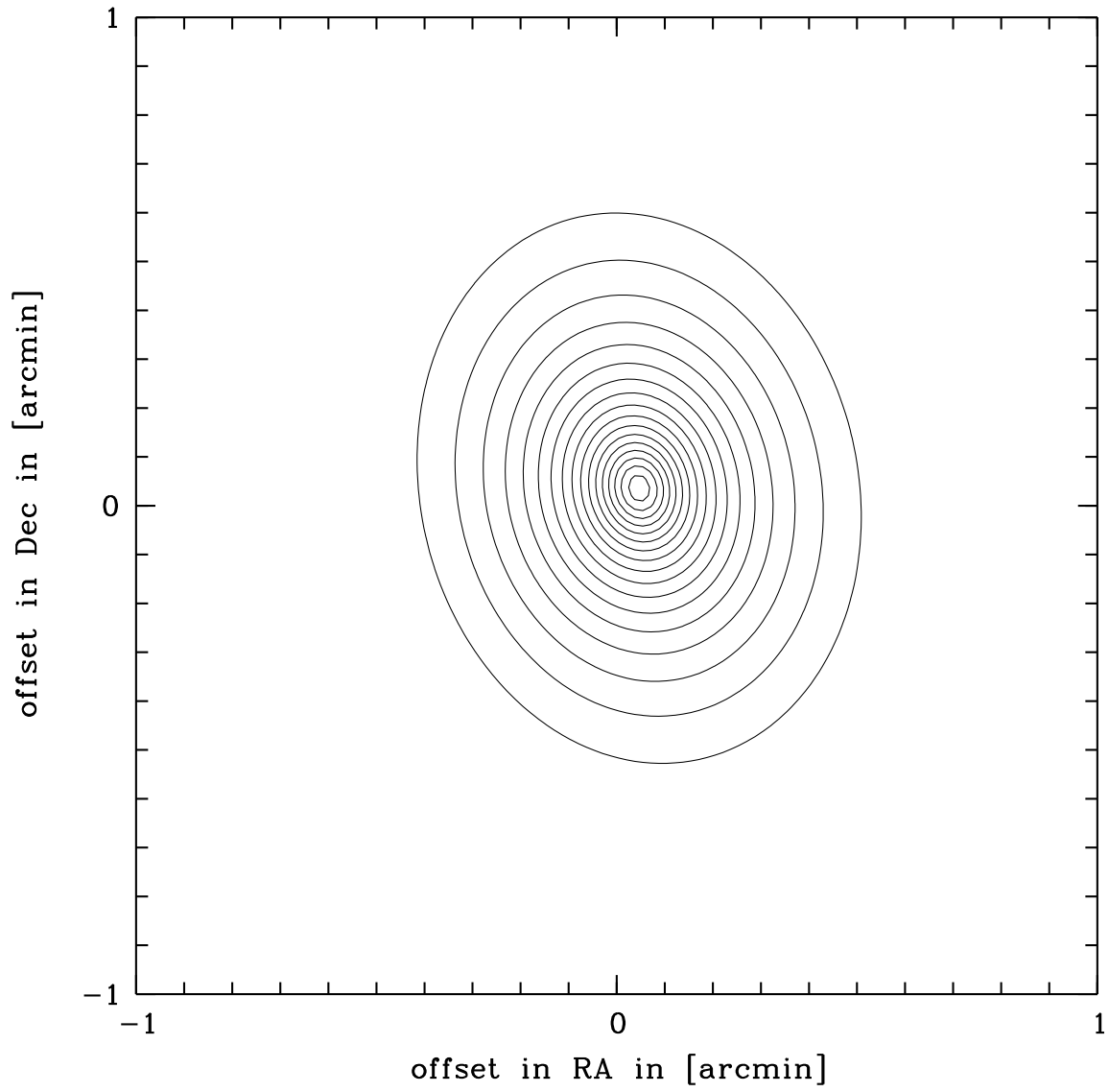


Fig. 3.—

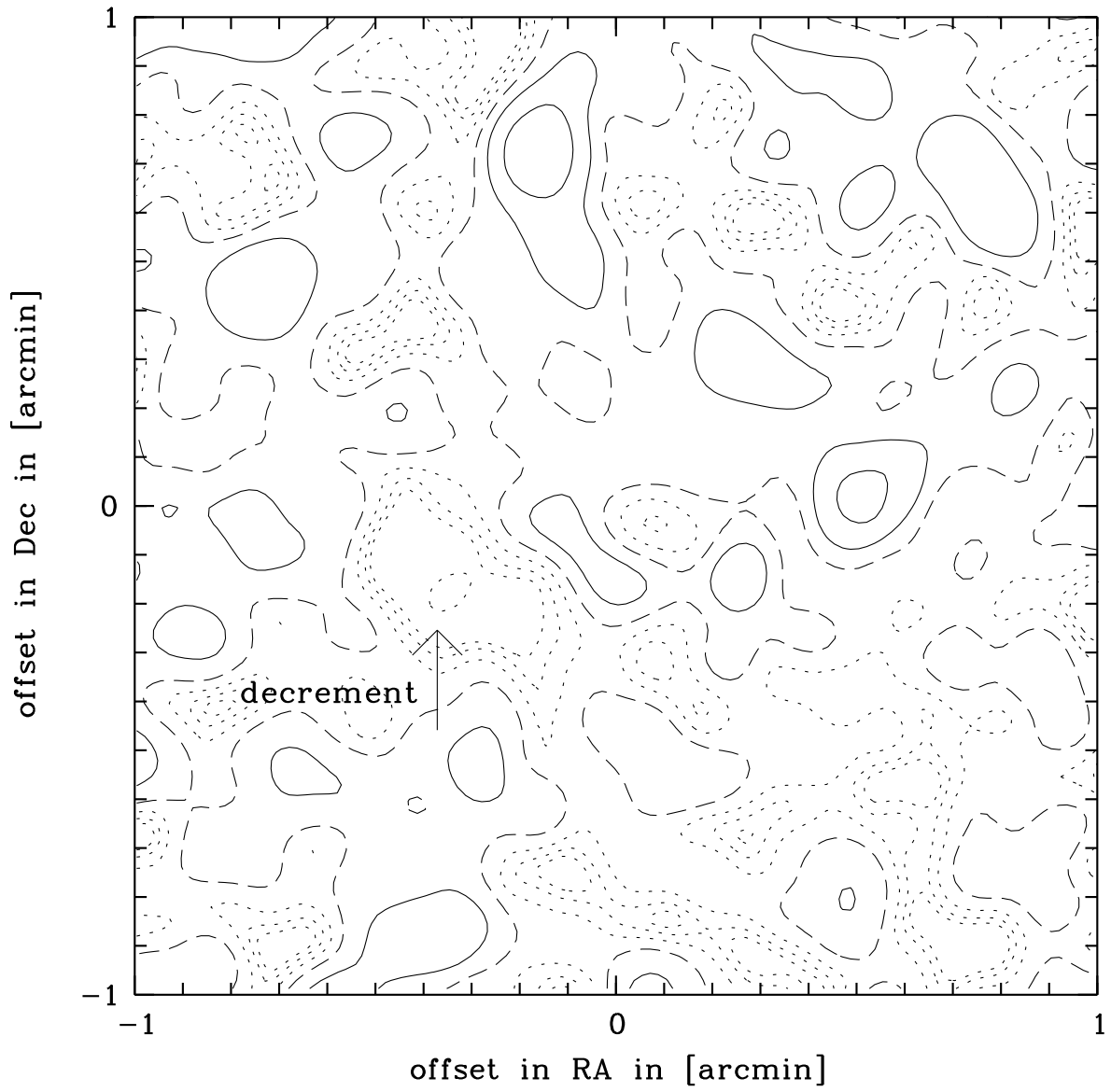


Fig. 4.—

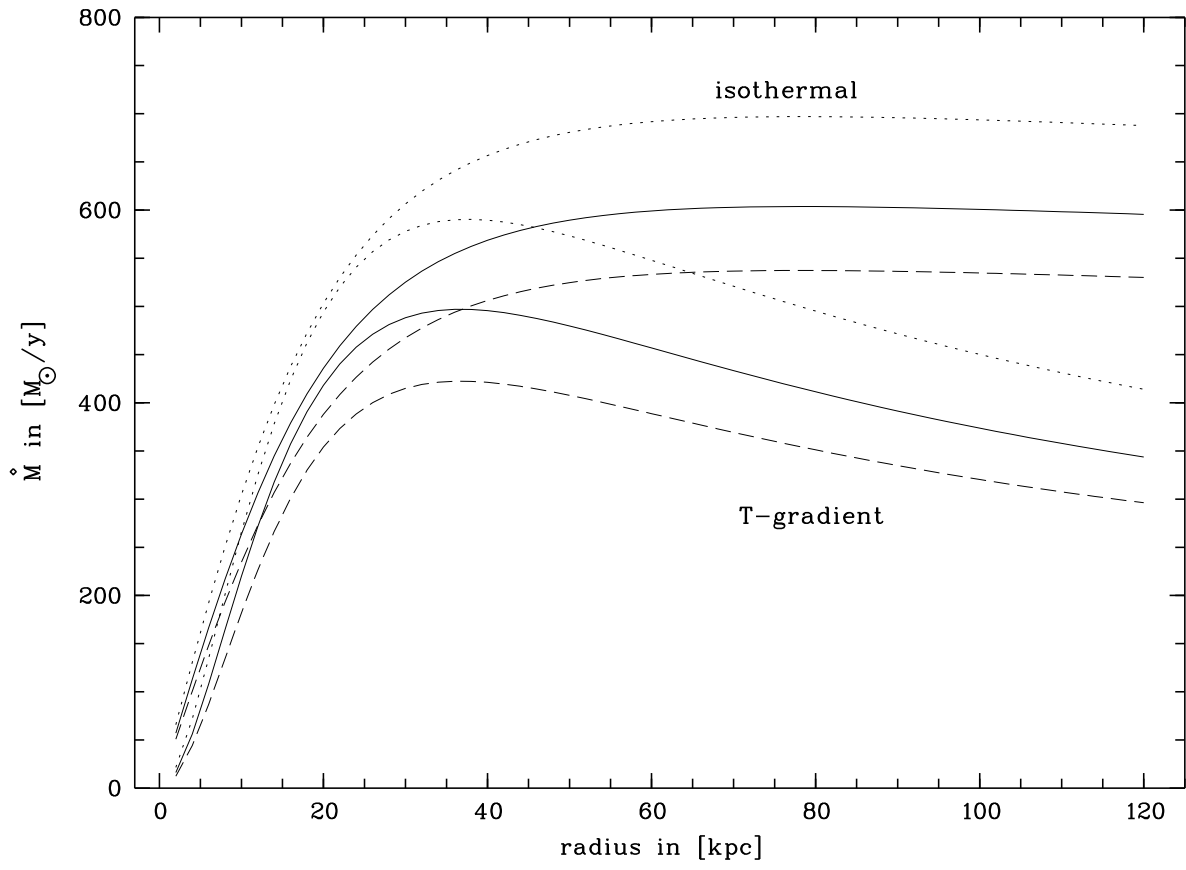


Fig. 5.—

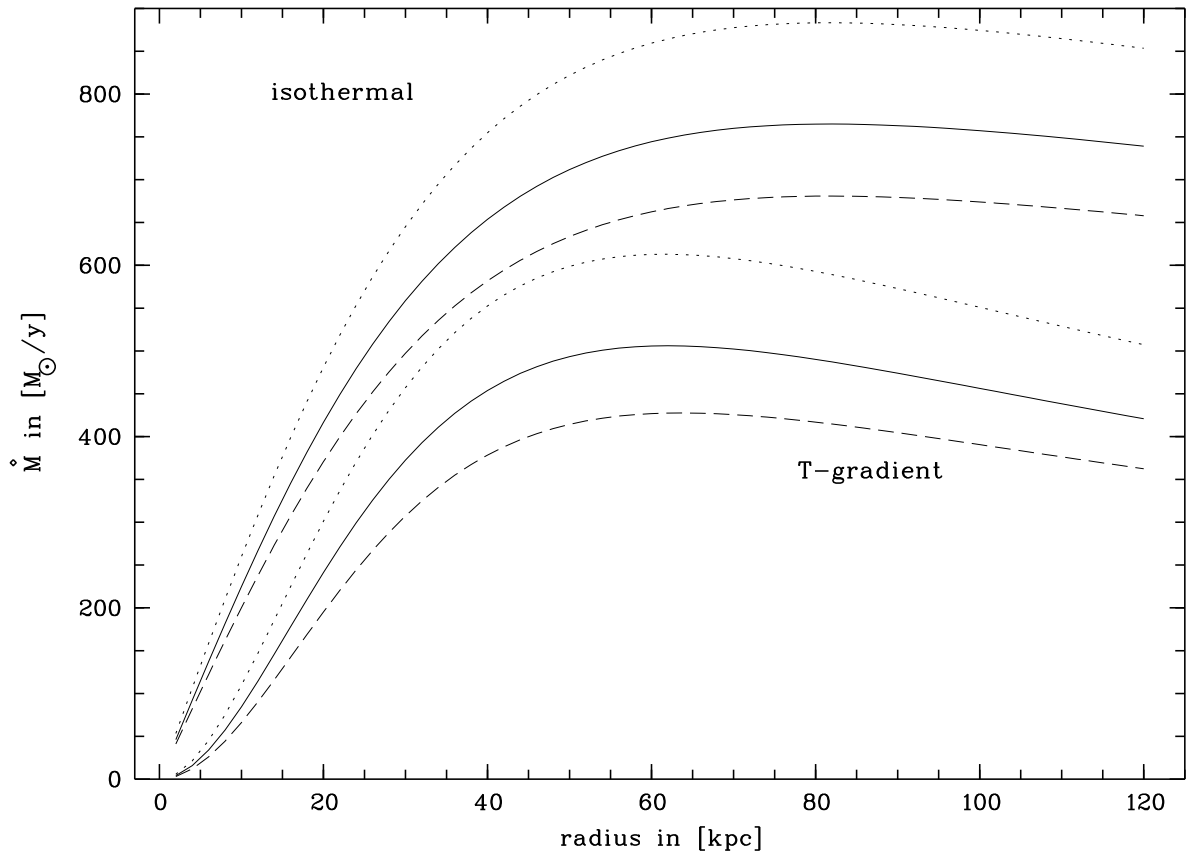


Fig. 6.—

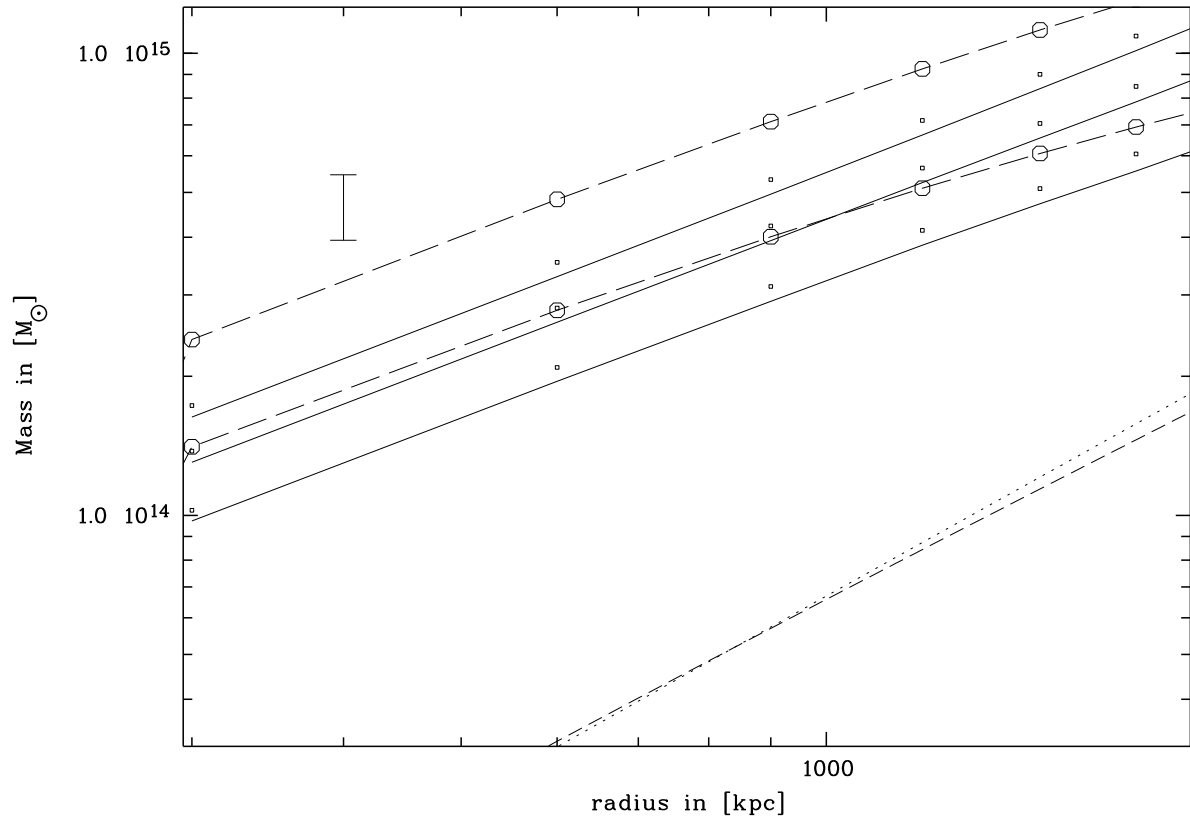


Fig. 7.—